

## Regional Lineament Pattern and Morphotectonic Analysis: The Investigation of Geological Structures and Present-Time Relative Tectonic Activity in the Tin Granite Area of Belitung Island, Indonesia

Harnanti Y. Hutami<sup>1\*</sup>, Nur Ayu Anas<sup>2</sup>, Erlangga I. Fattah<sup>1</sup>

<sup>1</sup>Geophysical Engineering Department, Faculty of Industry and Technology, Institut Teknologi Sumatera 35365, Indonesia

<sup>2</sup>Geological Engineering Department, Universitas Cendrawasih, Papua, Indonesia

\*Corresponding author. Email: [harnanti.hutami@tg.itera.ac.id](mailto:harnanti.hutami@tg.itera.ac.id)

Manuscript received: 14 March 2024; Received in revised form: 24 April 2024; Accepted: 28 April 2024

### Abstract

Belitung Island is located on the East Coast of Sumatra and is the southernmost extension of the Southeast Asian granite belt. Despite the flat terrain of the island, numerous granite outcrops provide insight into the past tectonic activities that caused the uplift in the region. This study analyzes the current state of Belitung's tectonic activity by examining its morphotectonic index and lineament pattern. A National Digital Elevation Model (DEMNAS) dataset with a resolution of up to 8.1 m will be used to assess the geological patterns and relative tectonic activity from the surface. The relationship between the regional lineament system and morphotectonic quantification throughout the landforms of Belitung Island will also be considered. The modified Segmented Tracing Algorithm (m-STA) technique extracted the lineament features. The Index of Relative Active Tectonic (IATR) was calculated by averaging several morphotectonic indices, such as asymmetry factors (AF), stream-length index (SL), mountain-front sinuosity (Smf), and valley floor width-height ratio (VF) factors, to quantify the relative tectonic activity of the area. The combination of the two methods shows that Belitung is currently experiencing relatively weak tectonic activity compared to the past. This is supported by the surface appearance, which is mainly composed of lowlands. Several granite outcrops and highlands are aligned along the NW-SE and NE-SW directions, corresponding to the main geological structures in the area.

**Keywords:** lineament; morphotectonic index; relative tectonic activity; structural geology.

**Citation:** Hutami, H. Y., Anas, N. A., and Fattah, E. I. (2024). Regional Lineament Pattern and Morphotectonic Analysis: The Investigation of Geological Structures and Present-Time Relative Tectonic Activity in the Tin Granite Area of Belitung Island, Indonesia. *Jurnal Geocelebes*, 8(1): 83–97, doi: 10.20956/geocelebes.v8i1.33887

### Introduction

Earth's surface morphology reflects the interaction between the rock and its geomorphological processes (Bishop, 2007). This concept has been one of the early targets for a better understanding of topographic features at the Earth's surface geological processes (Goudie, 2004). The attributes upon the Earth's surface have all the profound significance of their present and earlier chapters' conditions. A reciprocal relationship between tectonic activity and the geomorphological response of Earth's surface allows us to evaluate

current deformation processes due to the geological structures within the region (Goudie, 2004; Laake, 2022).

The interpretation of remote sensing data helps evaluate the geometry and landform variation of the earth's surface, which implies the structural, depositional, and erosional aspects (Laake, 2022). The continuously modified landforms are quantified using a set of geomorphic indices and are directly related to the active tectonic deformation (Zhazhalayi & Surdashy, 2022).

Despite the thickness of the sedimentary cover, lineaments are initially described as significant lines in the earth's face and later concluded as lines in the landscape that reveal the hidden architecture of the deep layers of rocks (Florinsky, 2016). The concept delineates geological lineaments, such as lithological boundaries, faults, fractures, and joints, caused by tectonic activities and geomorphological processes in terms of topographical lineaments (Ahmadi & Pekkan, 2021).

Belitung is located on the East Coast of Sumatra and is recognized as the southernmost continuation of the Southeast Asian granite belt through which the Bentong-Raub suture extends from Peninsular Malaysia. However, the extent of the suture extension is still not identified in this area due to a lack of supporting data (Wang et al., 2021; Zhang et al., 2023). Zhang et al. (2023) conducted a study on the correlation of the Bentong-Raub suture in the Bangka-Belitung Islands using information on granitic rocks and their ages to investigate this. Wang et al. (2021) estimated the types of granite distributed along the suture line, including Bangka and Belitung. They obtained their results using U-Pb geochronological, petrologic, elemental, and Sr-Nd-Pb-Hf isotopic studies. The findings indicate that the granite types found in the Bangka Belitung Islands belong to the Main Range Granite Province. Some granitoid formations on Belitung Island include Tanjungpandan Granite, Baginda Adamelite, Burungmand Granodiorite, and Batubesi Granite. Each of these formations is believed to have formed during different tectonic phases based on the mineral elements present in them (Lehmann & Harmanto, 1990).

A comprehensive investigation was conducted to unveil the tectonic evolution of Belitung Island. The study relied on the analysis of geochemical and petrographic data. The findings revealed that the Tanjungpandan and Batubesi granites were

formed during the syn-collision period between the Sibumasu and Indochina plates in the Late Triassic era. Conversely, the Baginda Adamelite and Burungmandi Granodiorite were formed during the post-collision tectonic phase that persisted until the Early Cretaceous period (Baharuddin & Sidarto, 1995). The Tanjungpandan granite outcrop area features a distinctive terrain shaped by morphotectonics, influenced by the underlying geological structure and tectonic movements. The lofty hills and scattered boulders within the formation offer evidence for this phenomenon. Concerning geomorphology analysis in granitic zones, a quantitative morphometric and morphotectonic analysis was carried out on river drains within moderately elevated granitic terrain and low-lying alluvium country. This revealed that the type of lithology and rock resistance affects the deformation of granitic terrain, as sedimentary rocks are more deformed than granitic rocks (Bhatt et al., 2020; Manjare, 2020).

Belitung Island is commonly classified as part of Sumatra Island, which has a history of tectonic activity due to the Sumatran Fault Systems and the closure of the Paleotethys Sea that led to the formation of the Bentong-Raub suture. Despite the island's relatively flat terrain, numerous granite outcrops offer a fascinating glimpse into the past tectonic activities that caused the granitoid uplift in the region. Additionally, the geological structures associated with the Sumatran faults system and Bentong-Raub suture may have intersected with the region, resulting in landform variations. As depicted in Figure 1, the area's higher terrain aligns with the main structures' NW-SE and NE-SW trends.

The area's geological formations and recent tectonic movements have yet to be analyzed in-depth. Although surface traces are not well-preserved, we believe past geological structures and tectonic episodes are

responsible for landform variation. The shrinkage of granite and the elevated topographic section at the center of the area are significant indicators of these changes. It is vital to develop approaches that can provide an initial estimate of potential geological structures that influence the landform changes up to the present time. This study aims to delve into the current

state of Belitung's tectonic activity, analyzing its morphotectonic index and lineament pattern to gain insights into the related structural geology. The results of this analysis will provide valuable information to better understand the area's geological structures and landform changes.

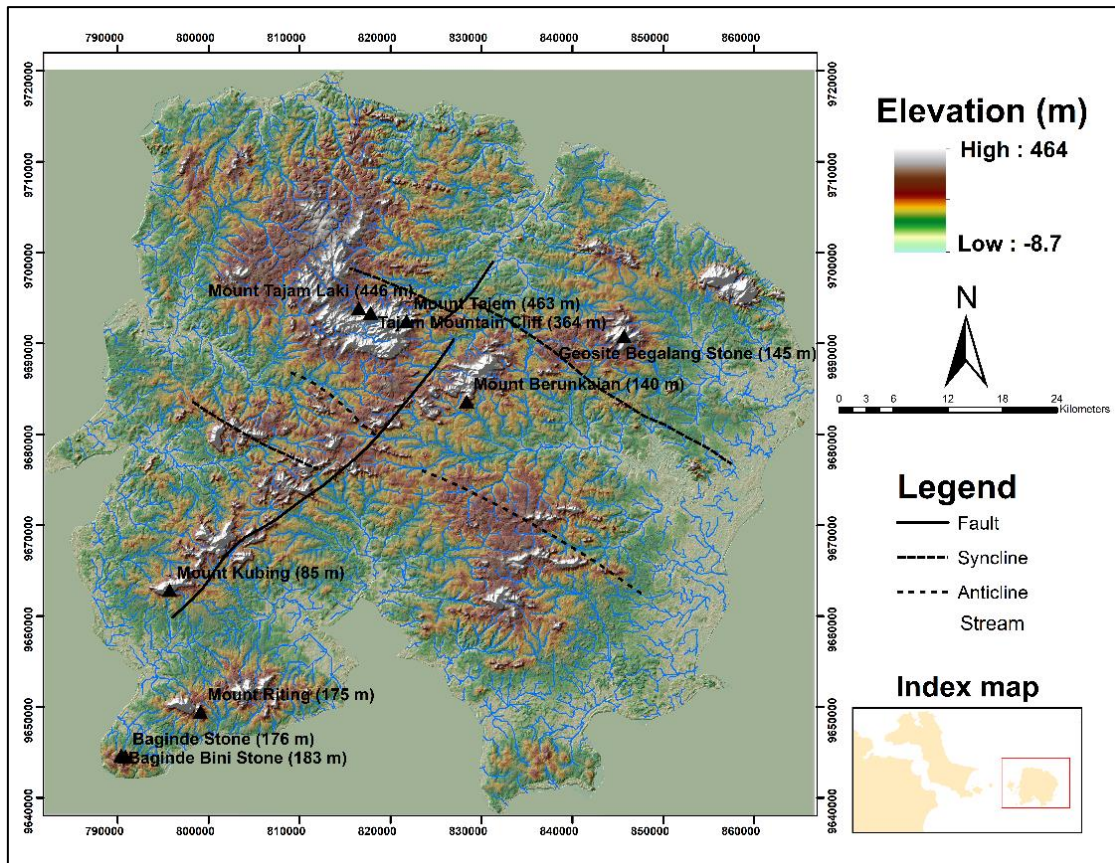


**Figure 1.** The map shows the variations of topographic levels in the study area.

#### *Geology summary of the study area*

Previous investigations have shown that the tectonic evolution of the Bangka-Belitung islands, to which Belitung belongs, has been influenced by the movement of the continental crust of the Sunda Shelf during oroclinal bending. Belitung Island's tectonic activity has significantly shaped its current morphological conditions (Zahirovic et al., 2014). In the Middle Triassic - Early Jurassic, magmatism formed granitoid spread along the western part of the Bukit Barisan and the Tin Islands (Bangka-Belitung Islands). The granitoid

originated had an absolute age of around 250 - 143 million years with an average age of approximately 220 million years with the formation of the tectonic order, including post-collision (Cobbing et al., 1986). The peak of magmatism in Peninsular Malaysia and the Tin Islands is at 220 million years, with the emergence of older granitoid in the Tin Islands (Barber & Crow, 2009; Cobbing et al., 1986; Lehmann & Harmanto, 1990).

The tectonic process on Belitung Island began with flysch sedimentary deposits from the Kelapakampit Formation (PCKs)

and the collision that formed the Siantu Formation (PCsv) in the form of alkaline igneous rock (lava) and breccias during the Permian-Carboniferous periods. The main magmatism activity occurred during the Triassic-Cenozoic periods. The formation of horst and graben parallel to the orogenic axis within this period happened due to a collision between the Sibumasu-Gondwana and Indochina blocks. This extensional tectonic arrangement led to the formation of the granite Main Range Province and Eastern Province in the Southeast Asian granite belt (Ng et al., 2017; Usman, 2016).

The recorded magmatism processes on Belitung Island are associated with the appearance of the Tanjung Pandan Granite Formation (Trtg), which contains primary cassiterite in the Triassic. The Tanjung Pandan granites in the northwest corner of Belitung Island is the largest igneous intrusion outcropped area consisting mainly of biotite granite, with a separate, minor quartz syenite sub-unit (Lehmann & Harmanto, 1990). The granite intrusion episodes had succeeded in breaking through sedimentary rocks, producing fractures in granite. In the Early Jurassic, the magmatic process was still ongoing and made the Adamelite Baginda (Jma) intrusion, which did not contain cassiterite.

The last magmatic process occurred in the Late Cretaceous, marked by diorite of Batubesi Formation (Kbd) and granodiorite of Burungmandi Formation (Kbg) intrusion. In the Late Cretaceous to the Quaternary, the dominant methods are erosion and deposition, which produce sand-carbonate deposits (Qpk) and alluvium (Qa) (Baharuddin & Sidarto, 1995). Structures that occurred in this area are folds, faults, joints, and lineaments. The direction of axial folds is NW-SE, and the

faults are trending NE-SW (Baharuddin and Sidarto, 1995).

## Materials and Methods

We aim to employ a National Digital Elevation Model (DEMNAS) dataset with a resolution of up to 8,1 m to assess the geological patterns and relative tectonic activity from the surface while considering the relationship of the regional lineament system and morphotectonic quantification throughout the entire landforms of the Belitung Island.

### *Linear features extraction*

We utilized remotely sensed data from the National Digital Elevation Model (DEMNAS) and geological maps of Belitung Island (1:250,000) to analyse the tectonic impacts and structural trends of the nineteen sub-watersheds of the interest area.

This study employed a modified Segmented Tracing Algorithm (m-STA) to extract geological linear features more accurately and efficiently. The m-STA is a highly sensitive and effective tool that leverages SAR backscattering intensity images to detect lines from pixels read as vector elements by analyzing local variations in the gray level of digital numbers (Army & Saepuloh, 2020; Saepuloh et al., 2018). The main objective of this approach was to identify surface geological structures by taking advantage of the dual orbit mode of Sentinel-1. To this end, backscattering intensity images of Phased Array type-L Synthetic Aperture Radar (PALSAR) from the Advanced Land Observing Satellite (ALOS) were also utilized, as detailed in Table 1. The dual orbit mode, comprising the ascending and descending modes, is illustrated in Figure 2.

**Table 1.** Information of data utilized for lineament extraction.

| Orbital Modes | Data         | Acquired Time   | Polarisation |
|---------------|--------------|-----------------|--------------|
| Ascending     | ALOS PALSAR  | 6 November 2010 | HH/HV        |
| Descending    | Sentinel 1-A | 7 November 2022 | VV/VH        |

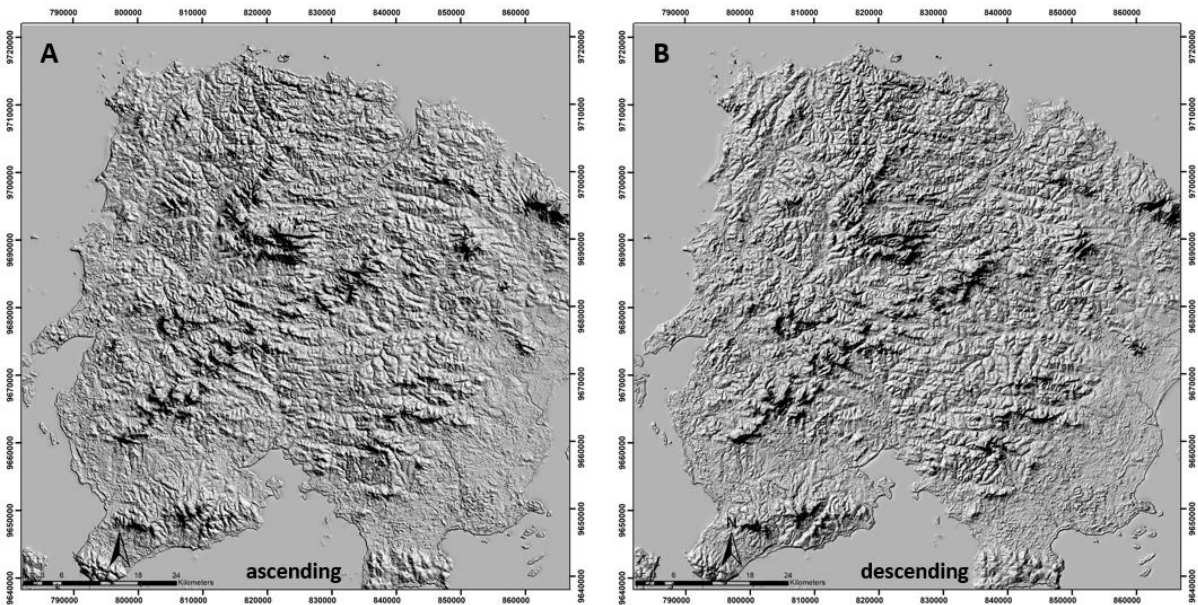


**Figure 2.** The dual orbital mode of ascending (A) and descending (B) for the study area with the detailed information listed in Table 1.

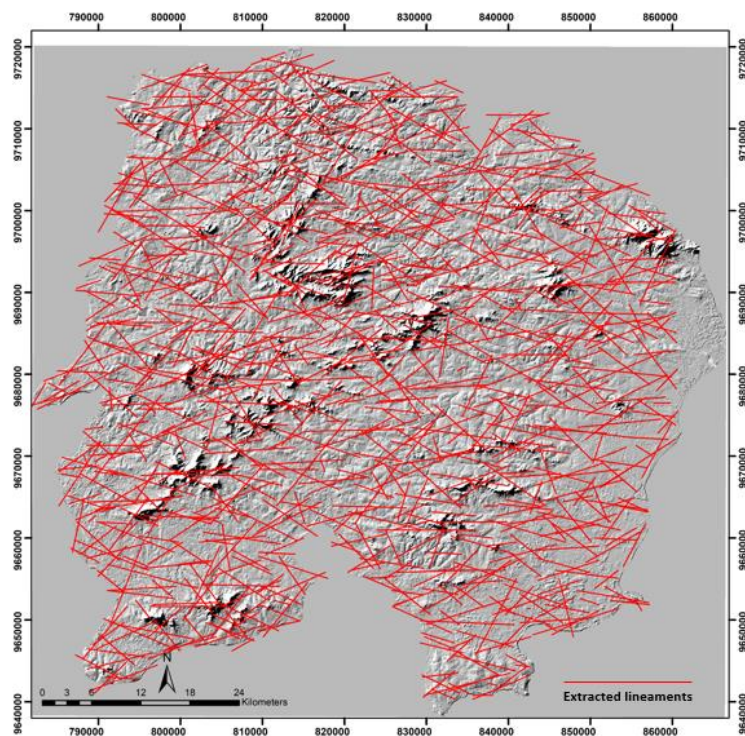


**Figure 3.** The extracted lineaments for the combined dual orbital modes of the study area.

This study used an automated process to extract lineaments from ascending and descending images, according to Saepuloh et al. (2018). The process had two main steps. The first step involved preparing the images through three stages: multi-looking, speckle filtering, and geometric correction. Multi-looking helped to increase the focus

without sacrificing resolution, speckle filtering minimized noise from surrounding objects, and geometric correction corrected any distortions caused by topographic variations or radar inclination. These steps were crucial for the m-STA application.

The second step involved identifying line elements by examining local variation along 16 directions, with  $11.25^\circ$  intervals within a small  $11 \times 11$  pixels window size. This was done by following the principle of STA. The segments were then transformed into a lineament by selecting a search ellipsoid window along a target segment whose start and middle points were inside the window with angle differences from the segment less than  $11.25^\circ$ . Segments that only had endpoints inside the window were excluded. The window size was determined by considering the agreement of the lineaments and major fault lengths in the study area.

Finally, one line was defined as a lineament by approximating the coordinates of the start and end points of the selected segments using the least squares method. The lineaments from the ascending and descending mode images were merged, and the overlaps were grouped into one line using the least square method, as shown in Figure 3.

#### *Morphotectonic index quantification*

The morphotectonic variables were calculated using each equation in Table 2, and our geomorphological analysis was grouped into two categories: drainage basin-based and mountain front-based: the drainage basin-based analysis calculated asymmetry factors (AF) and stream-length index (SL). In contrast, the mountain front-based analysis included mountain-front sinuosity (Smf) and valley floor width-height ratio (VF) factors.

The Asymmetry Factor (AF) Index is used to assess whether there is tectonic tilting at the scale of a drainage basin. The index values are most effective when applied to drainage basins with the same underlying rock type if neither lithologic controls nor localized climate affects the level of asymmetry (Green, 1997), which was calculated using Equation 2.

The SL index is calculated (Equation 3) to analyze the relationship between episodes of tectonic activity, which relatively changes the slope gradient and length of streams, rock resistance to erosion processes, and thus the study area's surface topography (Kumar et al., 2022).

The VF index differentiates between the broader-floored canyons of U-shaped valleys with higher VF and the relatively lower values of VF, which indicates the V-shaped valleys. The U-shaped valleys are associated with slower tectonic and uplift activities so that the streams may cut broad the valley floors. Low VF values reflect the more profound valleys with streams actively incising and commonly associated with the uplift. Each VF value throughout the segmented sub-watersheds is calculated using Equation 4 from Table 2 to get detailed values of VF.

Tectonic activity, which is mainly horizontal crustal movement, causes deformation in the Earth's surface, resulting in the formation of mountains. The shape of a mountain face can indicate the type of tectonic activity occurring in a particular area. For instance, mountain faces in regions with primarily compressive tectonic activity tend to be relatively straight. Conversely, mountain faces are often more winding or curved in areas with extensional tectonic activity. This is because extensional activity leads to the formation of valleys and depressions between mountain ranges, which can result in undulating or tortuous mountain faces (Eleni et al., 2015; Partabian et al., 2016).

Mountain Front Sinuosity (Smf) is an index used in morphotectonics to understand the geomorphological processes that lead to the formation of mountain faces. The index is a ratio of the mountain front length along the mountain's foot (Lmf) to the straight-line distance of the mountain front (Ls). The lower values of Smf, associated with the active tectonic and uplift, are shown as

straight mountain fronts. If this uplift rate ceases, the erosional processes tend to be more dominant and carve irregular mountain fronts, presented by the relatively higher value of Smf.

These indices have been proven to be effective tools in examining landform processes due to tectonic implications (Andrifa et al., 2021; Eleni et al., 2015; Gentana et al., 2018; Gupta et al., 2022; Shiran et al., 2020).

**Table 2.** The morphotectonic parameters to evaluate the relative tectonics of Belitung Island, Indonesia.

| Morphotectonic indicators                   | Mathematical expression  | Class ranges adopted in the study  | References   |
|---|--|--|--|
| <b>Asymmetry factor (AF)</b>                | $AF = (A_r/A_t) \times 100$ (1)  | <b>Class 1</b> (high tilting): AF>65 or AF<35<br><b>Class 2</b> (moderate tilting): 57<AF<65 or 35<AF<43<br><b>Class 3</b> (low tilting): 43<AF<57                                 | (Eleni et al., 2015; Green, 1997; Luirei et al., 2021; Partabian et al., 2016) |
| <b>Stream-length gradient index (SL)</b>    | $SL = (\Delta h/\Delta l) \times L$ (2)                                      | <b>Class 1</b> (high active tectonic): SL > 500<br><b>Class 2</b> (moderately active tectonic): 300 < SL < 500<br><b>Class 3</b> (low active tectonic): SL < 300                   |  |
| <b>Mountain-front sinuosity (Smf)</b>       | $Smf = L_{mf}/L_s$ (3)   | <b>Class 1</b> (active tectonic): Smf 1.2-1.6<br><b>Class 2</b> (intermediate-to-low active tectonic): Smf 1.8-3.4<br><b>Class 3</b> (tectonic inactive): Smf 2.0-7.0              |  |
| <b>Valley floor width-height ratio (VF)</b> | $VF = \frac{(2 \times V_{fw})}{[(E_{ld} - E_{sc}) + (E_{rd} - E_{sc})]}$ (4) | <b>Class 1</b> (highly uplifted with V-shaped valley): Vf < 0,5<br><b>Class 2</b> (moderately uplifted): Vf 0.5-1<br><b>Class 3</b> (lowly uplifted with a U-shaped valley): Vf >1 |  |

**Results**

*Geological lineament pattern*

The depicted rosette diagram in Figure 4 shows that linear surface features in the study area have at least three preferred orientations: NW-SE, NE-SW, and relatively E-W and ESE-WNW. The first two trends agreed with the direction of existing faults and folds mapped in the same direction, indicating synthetic and antithetic strike-slip faults developed within the study area (Baharuddin & Sidarto, 1995). However, the WSW-ENE axis pattern obtained from this study hypothetically informs us of a new pattern in the island region, which is presumed to

be related to the extension of the Bentong-Raub suture.

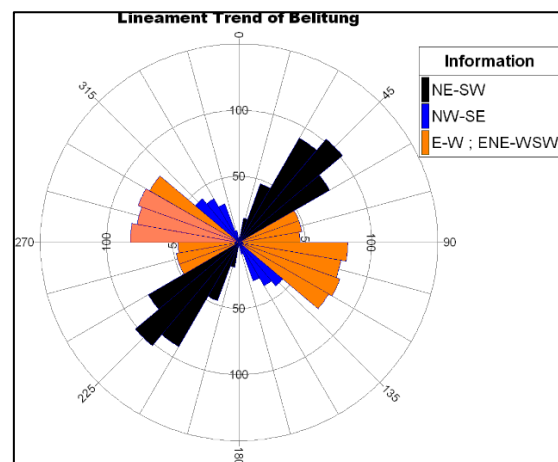


**Figure 4.** Rosette diagram showing linear surface trends of geological features identified from the lineament extraction.

*Response of the morphological indicators regarding tectonic activity*

According to the Smf values calculated for the 19 sub-watersheds (as seen in Figure 5), Belitung falls under the category of "Inactive Tectonics" with values ranging from 2–7, while the remaining sub-watersheds indicating lower-to-moderate category with values ranging from 1.8 – 3.4. Additionally, the Asymmetry Factor (AF) was calculated to determine the degree of slope or asymmetry of geological features, and it revealed that each correlated formation in Belitung falls under a different class. The higher tectonic class category is represented by sub-watersheds (1), (5), (16), and (18), with AF values ranging from 30-55. In contrast, other sub-watersheds have been classified under moderate and lower tectonic classes, represented by classes 2 and 3, respectively. The overall results of the AF and Smf value calculations are presented in Table 3.

The stream length gradient (SL) index is another factor when assessing tectonic activity. It examines the relationship between the geological structure and the shape of the drainage network. Generally, higher SL values in an area indicate an uplift marked by steeper slopes and faster river flow. Conversely, lower SL values suggest a more stable landscape with slower water transport. Belitung's SL values for 15 sub-watersheds fall into class 2, including sub-watersheds (1), (2), (3), (7), (8), (10), (16), (17), (18), and (19), while the other five belong to tectonic class 3 (Figure 6A).

The VF factor is crucial for identifying active tectonic activity in each area. This is based on the type and amount of tectonic activity. Figure 6B provided the VF value for each sub-watershed segment, and the spatial distribution shows the average result. The VF values in the Belitung area fall into three intervals: 2,286-17,175 (interval 1), 17,176-32,066 (interval 2), and 32,006-46,957 (interval 3). According to

the reference, Belitung has a low uplift level (class 3), with a predominantly U-shaped valley.

Next up for analysis is averaging the Smf, AF, VF, and SL values for all sub-watersheds, which is the Index of Active Tectonic Relative (IATR). This index represents a summary and average of the given geomorphic indices which are used in the study and can be obtained using the equation:

$$IATR = S/N \quad (5)$$

S represents the sum of previous indices, and N represents the number of selected indices. This IATR quantified the active tectonic relative throughout the study area in terms of their classifications (Mahmood & Gloaguen, 2012). The values of the index were divided into four classes to define the degree of active tectonics: Class 1—very high ( $1.0 \leq IATR < 1.5$ ); Class 2—high ( $1.5 \leq IATR < 2.0$ ); Class 3—moderate ( $2.0 \leq IATR < 2.5$ ); and Class 4—low ( $2.5 \leq IATR$ ) (Gentana et al., 2018; Green, 1997).

This technique has been applied to several objectives, such as identifying the geomorphic indices changes within the fault system with the most seismic and motional potential (Eynoddin et al., 2017), the tectonic activity along the uplifted anticline zones that has resulted in various surface landforms (Othman & Omar, 2023; Partabian et al., 2016), and from the regional Indonesia area was the assessment for developing geological disaster-based area in Karangsambung geopark (Hidayat et al., 2023). These resulted in proper analysis that higher IATR corresponded to the higher impacted tectonic activity or most changed landforms, such as uplifted land, fault/ fracture traces, etc., in the study area (Figure 7).

Table 4 provides the IATR values for each sub-watershed in Belitung, which falls into the tectonic class 3 and 4 categories, suggesting a relatively low to medium level of tectonic activity in the present time.

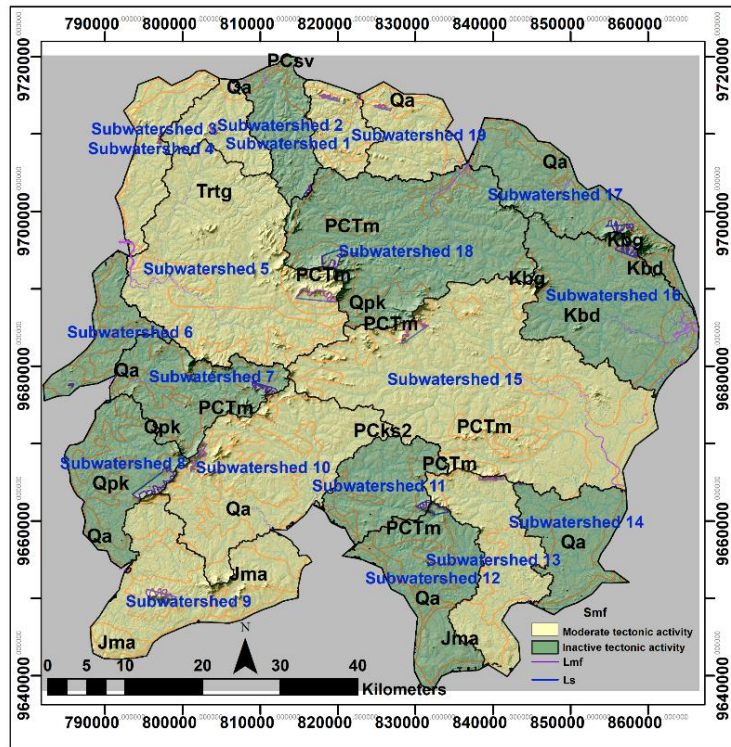


Figure 5. Map showing the spatial distribution of the Smf index regarding their calculated values.

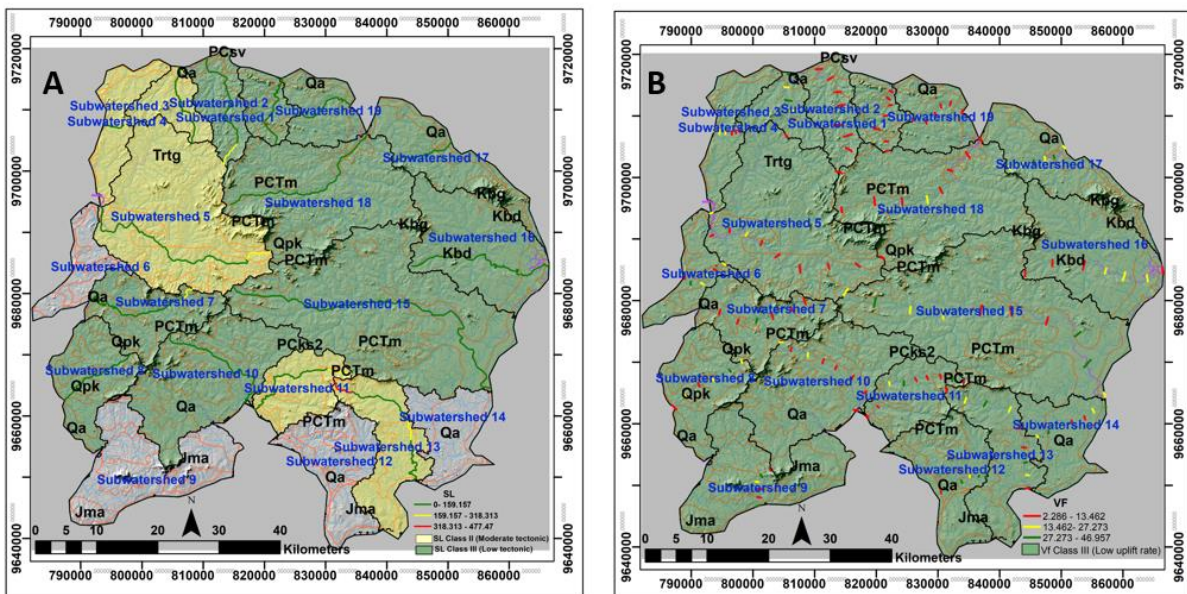
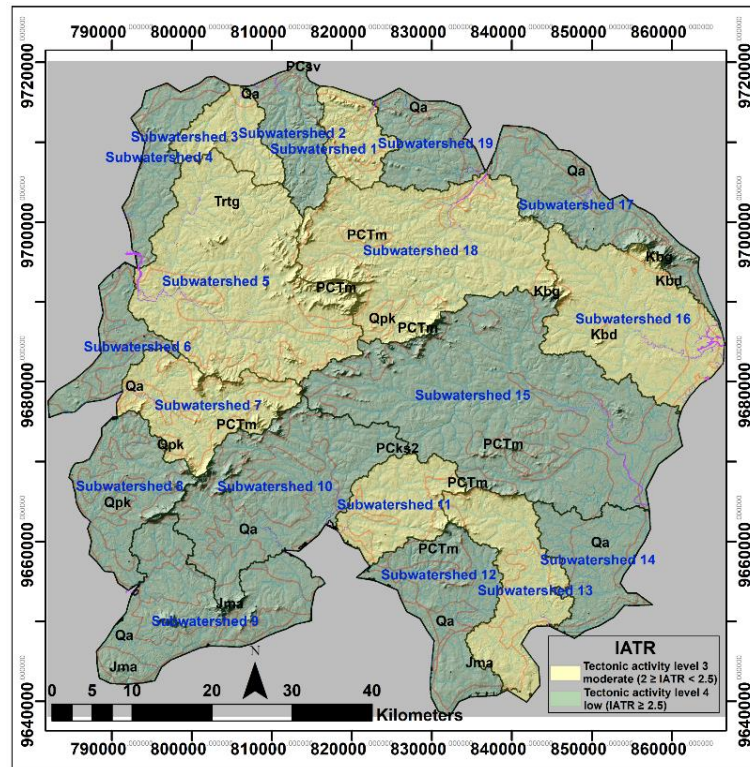


Figure 6. The spatial distribution of SL (A) and VF (B) regarding their classification.

*Discussion*

Over the years, Belitung Island has undergone significant tectonic activity, giving rise to various rock formations such as the Kelapakampit Formation, Siantu Formation, Tanjungpandan Granite outcrops, Baginda Adamelit, Burungmandi Granodiorite, and Batubesi Granite.

Through analysis of the morphotectonic index, Belitung falls within a very low tectonic classification. This is due to the prevailing effects of erosion and denudation in the region, which limit the range of surface elevation needed to calculate key indices like Smf, AF, VF, and HI.



**Figure 7.** Map showing the spatial distribution of IATR in Belitung Island, Indonesia.

However, Sub-watersheds (1) and (5) in Belitung Island's northern region, where granitic intrusions from the Tanjungpandan Formation are present, exhibit higher AF values than other regions. Likewise, sub-watersheds (16) and (18) have AF values linked to the Kalapa Kampit Formation (PCKs) in the form of Flysch sediments weakly to moderately folded. These AF values represent the higher variation of these sub-watersheds asymmetry/ tilting slope and correlate to the higher tectonic level.

Moreover, analysis of the SL and VF indices reveals tectonic classes ranging from weak to medium. SL values were derived solely from 15 sub-watersheds located in Belitung, utilizing their primary drainages. The SL index highlights a notable value discrepancy between sub-watersheds 11 and 13, distinguished by their steeper river slopes. It can be inferred that the study area exhibits low-to-moderate tectonic activity based on the average values of AF, Smf, SL, and VF. These results brought our analysis to the

path that, as per Baharuddin and Sidarto (1995), different types of tectonic activities began approximately 300 million years ago during the Permo-Carbon Age, forming flysch sedimentary deposits and the fold system of the Kelapakampit Formation.

The tectonic activity of the study area continued with magmatic activity that produced the Tanjungpandan Granite in the Triassic period. The granite intrusion phenomenon succeeded in breaking through sedimentary rocks, which also produced fractures in the granite.

In the Early Jurassic period, magmatic activity continued and caused the breakthrough of the Baginda Adamelite rocks, which ended in the Late Cretaceous by producing diorite and granodiorite breakthroughs. The erosion and deposition occurred in the aftermath, producing carbonaceous sand deposits and alluvium. These granitoid types then underwent uplift or were exposed to the surface due to intensive erosion events that caused the granite cover layer to erode. As a result, granite rocks were exposed on the surface

during the Cenozoic period (Tertiary quarter). However, erosion and deposition during the Tertiary-Quaternary period have left their mark, exposing the island's granite rocks. Denudation and deposition in valleys have resulted in a nearly level plain.

The geomorphic indices spatial distribution shows that the quantified area along the main streams analyzed corresponds to the orientation of the main structure within the islands, so our investigation continues to trace geologic features from lineaments to delineate the potential traces of structures.

The lineament pattern suggests a similar orientation to that of the main fault system of Sumatra in the NW-SE and NE-SW directions. In the granite outcrop areas (sub-watersheds 1,2,3 and 4), lineaments may correspond to zones of differential weathering and fracturing within the granite, which can further influence the hill terrain. Additionally, minor lineament orientation in the ENE-WSE and E-W directions are believed to be related to the collision process between the East Malaya continental terrane and Sibumasu, forming a suture known as Raub-Bentong. This suture extends north-south and turns southeast into Indonesia, including Belitung Island (Lehmann & Harmanto, 1990; Zhang et al., 2023). During this period, a subduction event also produced the Siantu Formation of basic igneous rocks (lava) and breccia.

## **Conclusion**

The lineament analysis identified the dominantly NW-SE and NE-SW trending fault and fold, respectively. These two orientations have a strong correlation with the tectonic processes of Sumatra and the formation of the Sumatra Main Fault in the same direction. The other minor directions obtained are interpreted as part of the

Bentong-Raub suture that passes through Belitung and is presumed to continue westward toward Kalimantan Island.

The quantitative geomorphology indices assessment combined with the lineament analysis from the satellite imagery indicate that Belitung Island is in a state of relatively low tectonic activity, with the more uplifted landform concentrated along the Tanjung pandan granitoid outcrop that was produced in the Triassic period during the magmatic activity and Kalapakampit folded system. The analysis is supported by a class 1 high AF value of less than 35.

Finally, the IATR shows that relatively low-to-moderate tectonic activity is distributed to the northwest and mostly concentrated in the southeast region, corresponding to the fault and fold systems of the island, respectively.

## **Acknowledgments**

We thank Institut Teknologi Sumatra for supporting the study. Gratitude was also sent to this manuscript's reviewer, and everyone involved in the discussion informally.

## **Author Contribution**

Harnanti Y. Hutami worked on the concept of the text and whole data analysis. Nur Ayu Anas contributed to morphotectonic data interpretation and provided good figures. Erlangga I. Fattah interpreted the lineament features in the study area.

## **Conflict of Interest**

The authors declare that they have no known competing financial interests or personal relationships that could have appeared to influence the work reported in this paper article.

**Table 3.** The results of the asymmetry factor and sinuosity mountain front of the study area.

| Sub-watersheds | Asymmetry Factor (AF) |        |       | AF Class | Sinuosity Mountain Front (Smf) |       |      | Smf Class |
|----------------|-----------------------|--------|-------|----------|--------------------------------|-------|------|-----------|
|                | Ar                    | At     | AF    |          | Lmf                            | Ls    | Smf  |           |
| 1              | 24,54                 | 81,23  | 30,21 | 1        | 6,044                          | 2,669 | 2,26 | 2         |
| 2              | 47,87                 | 114,93 | 41,65 | 2        | 4,333                          | 1,613 | 2,69 | 3         |
| 3              | 39,17                 | 89,88  | 43,58 | 3        | 2,846                          | 1,405 | 2,03 | 2         |
| 4              | 65,40                 | 120,82 | 54,13 | 3        | 3,154                          | 1,553 | 2,03 | 2         |
| 5              | 148,79                | 527,05 | 28,23 | 1        | 10,711                         | 4,747 | 2,26 | 2         |
| 6              | 50,83                 | 99,65  | 51,00 | 3        | 1,428                          | 0,377 | 3,79 | 3         |
| 7              | 69,61                 | 188,20 | 36,99 | 2        | 10,836                         | 3,146 | 3,44 | 3         |
| 8              | 91,64                 | 180,30 | 50,83 | 3        | 16,126                         | 4,909 | 3,28 | 3         |
| 9              | 109,23                | 287,50 | 37,99 | 2        | 9,593                          | 3,900 | 2,46 | 2         |
| 10             | 133,95                | 370,40 | 36,16 | 2        | 9,031                          | 4,170 | 2,17 | 2         |
| 11             | 49,01                 | 137,95 | 35,53 | 2        | 5,229                          | 1,591 | 3,29 | 3         |
| 12             | 80,11                 | 207,10 | 38,68 | 2        | 5,664                          | 2,010 | 2,82 | 3         |
| 13             | 75,65                 | 204,20 | 37,05 | 2        | 6,993                          | 3,096 | 2,26 | 2         |
| 14             | 57,56                 | 148,25 | 38,83 | 2        | 1,712                          | 0,433 | 3,95 | 3         |
| 15             | 366,21                | 746,36 | 49,07 | 3        | 8,625                          | 4,138 | 2,08 | 2         |
| 16             | 102,23                | 317,48 | 32,20 | 1        | 12,314                         | 2,725 | 4,52 | 3         |
| 17             | 111,25                | 198,50 | 56,04 | 3        | 10,112                         | 3,53  | 2,86 | 3         |
| 18             | 153,40                | 459,14 | 33,41 | 1        | 8,092                          | 2,445 | 3,31 | 3         |
| 19             | 67,76                 | 122,39 | 55,36 | 3        | 4,311                          | 2,15  | 2,01 | 2         |

**Table 4.** Results of *IATR* Index Calculation according to geomorphic indices averaging values.

| Sub-watersheds | Smf | AF | Vf | SL | IATR | Class |
|----------------|-----|----|----|----|------|-------|
| 1              | 2   | 1  | 3  | 3  | 2.25 | 3     |
| 2              | 3   | 2  | 3  | 3  | 2.67 | 4     |
| 3              | 2   | 3  | 3  | 2  | 2.50 | 3     |
| 4              | 2   | 3  | 3  | 2  | 2.50 | 4     |
| 5              | 2   | 1  | 3  | 2  | 2.00 | 3     |
| 6              | 3   | 3  | 3  | *  | 3.00 | 4     |
| 7              | 3   | 2  | 3  | 3  | 2.75 | 3     |
| 8              | 3   | 3  | 3  | 3  | 3.00 | 4     |
| 9              | 2   | 2  | 3  | *  | 2.50 | 4     |
| 10             | 2   | 2  | 3  | 3  | 2.67 | 4     |
| 11             | 3   | 2  | 3  | 2  | 2.33 | 3     |
| 12             | 3   | 2  | 3  | *  | 2.50 | 4     |
| 13             | 2   | 2  | 3  | 2  | 2.33 | 3     |
| 14             | 3   | 2  | 3  | *  | 2.50 | 4     |
| 15             | 2   | 3  | 3  | 2  | 2.67 | 4     |
| 16             | 3   | 1  | 3  | 3  | 2.33 | 3     |
| 17             | 3   | 3  | 3  | 3  | 3.00 | 4     |
| 18             | 3   | 1  | 3  | 3  | 2.33 | 3     |
| 19             | 2   | 3  | 3  | 3  | 3.00 | 4     |

(\*) means no calculated values in this sub-watershed.

## References

- Ahmadi, H., & Pekkan, E. (2021). Fault-based geological lineaments extraction using remote sensing and GIS—A review. *Geosciences (Switzerland)*, 11(5), 183. <https://doi.org/10.3390/geosciences11050183>
- Andrifa, J., Sulaksana, N., Gentana, D., & Sulastris, M. (2021). Geological Lineament Pattern and Geomorphic Indices Characteristic Related To Geothermal Manifestation Appearance: A Case Study from Gunung Talang District and Its Surroundings, Solok Regency, West Sumatra Province, Indonesia. *International Journal of Scientific*

- Research in Science and Technology*, 8(3), 323–336. <https://doi.org/10.32628/ijrsrst218358>
- Army, E. K., & Saepuloh, A. (2020). Field Verifications of Geological Structures Related to SAR Detected Lineaments. *IOP Conference Series: Earth and Environmental Science*, 417(1), 012012. <https://doi.org/10.1088/1755-1315/417/1/012012>
- Baharuddin, & Sidarto. (1995). *Peta Geologi Lembar Belitung, Sumatera (1:250,000)*. Puslitbang Geologi, Indonesia. <https://geologi.esdm.go.id/geomap/pages/preview/peta-geologi-lembar-belitung-sumatera>
- Barber, A. J., & Crow, M. J. (2009). Structure of Sumatra and its implications for the tectonic assembly of Southeast Asia and the destruction of Paleotethys. *Island Arc*, 18(1), 3–20. <https://doi.org/10.1111/j.1440-1738.2008.00631.x>
- Bhatt, S. C., Singh, R., Ansari, M. A., & Bhatt, S. (2020). Quantitative Morphometric and Morphotectonic Analysis of Pahuj Catchment Basin, Central India. *Journal of the Geological Society of India*, 96(5), 513–520. <https://doi.org/10.1007/s12594-020-1590-1>
- Bishop, P. (2007). Long-term landscape evolution: linking tectonics and surface processes. *Earth Surface Processes and Landforms*, 32, 329–365. <https://doi.org/10.1002/esp.1493>
- Cobbing, E. J., Mallick, D. I. J., Pitfield, P. E. J., & Teoh, L. H. (1986). The granites of the Southeast Asian Tin Belt. *Journal of the Geological Society*, 143(3), 537–550. <https://doi.org/10.1144/gsjgs.143.3.0537>
- Eleni, K., Skilodimou Hariklia, D., Bathrellos George, D., Assimina, A., & Evangelos, K. (2015). Morphotectonic analysis, structural evolution/pattern of a contractional ridge: Giouchtas Mt., Central Crete, Greece. *Journal of Earth System Science*, 124(3), 587–602. <https://doi.org/10.1007/s12040-015-0551-3>
- Eynoddin, E. H., Solgi, A., Pourkermani, M., Matkan, A., & Arian, M. (2017). Assessment of Relative Active Tectonics in the Bozgoush Basin (SW of Caspian Sea). *Open Journal of Marine Science*, 07(02), 211–237. <https://doi.org/10.4236/ojms.2017.72016>
- Florinsky, I. V. (2016). Lineaments and Faults. *Digital Terrain Analysis in Soil Science and Geology*, 353–376. <https://doi.org/10.1016/b978-0-12-804632-6.00014-6>
- Gentana, D., Sulaksana, N., Sukiyah, E., & Yuningsih, E. T. (2018). Index of active tectonic assessment: Quantitative-based geomorphometric and morphotectonic analysis at Way Belu Drainage Basin, Lampung Province, Indonesia. *International Journal on Advanced Science, Engineering and Information Technology*, 8(6), 2460–2471. <https://doi.org/10.18517/ijaseit.8.6.6089>
- Goudie, A. S. (2004). Encyclopedia of Geomorphology. In *Encyclopedia of Geomorphology* (eBook). Taylor & Francis.
- Green, D. J. (1997). Active Tectonics Earthquakes, Uplift, and Landscape. *Environmental & Engineering Geoscience*, III(3), 463–464. <https://doi.org/10.2113/gseegeosci.iii.3.463>
- Gupta, L., Agrawal, N., Dixit, J., & Dutta, S. (2022). A GIS-based assessment of active tectonics from morphometric parameters and geomorphic indices of Assam Region, India. *Journal of Asian Earth Sciences: X*, 8, 100115. <https://doi.org/10.1016/j.jaesx.2022.100115>
- Hidayat, E., Muslim, D., Zakaria, Z., Permana, H., & Wibowo, D. A.

- (2023). Index active tectonic relative of Karangsambung geopark area, Central Java, Indonesia: assessment for developing geological disaster-based areas. *IOP Conference Series: Earth and Environmental Science*, 1173, 012014. <https://doi.org/10.1088/1755-1315/1173/1/012014>
- Kumar, N., Dumka, R. K., Mohan, K., & Chopra, S. (2022). Relative active tectonics evaluation using geomorphic and drainage indices, in Dadra and Nagar Haveli, western India. *Geodesy and Geodynamics*, 13(3), 219–229. <https://doi.org/10.1016/j.geog.2022.01.001>
- Laake, A. (2022). *Remote Sensing for Hydrocarbon Exploration* (Springer R). Springer. <https://doi.org/10.1007/978-3-030-73319-3>
- Lehmann, B., & Harmanto. (1990). Large-scale tin depletion in the Tanjungpandan tin granite, Belitung Island, Indonesia. *Economic Geology*, 85(1), 99–111. <https://doi.org/10.2113/gsecongeo.85.1.99>
- Luirei, K., Bhakuni, S. S., Longkumer, L., Kumar, V., & Jamir, I. (2021). Geomorphic assessment of the factors contributing to the evolution of landforms in Ukhaldhunga area, Kosi River valley, Kumaun Himalaya, Uttarakhand. *Geosciences Journal*, 25(4), 465–478. <https://doi.org/10.1007/s12303-020-0034-7>
- Mahmood, S. A., & Gloaguen, R. (2012). Appraisal of active tectonics in Hindu Kush: Insights from DEM derived geomorphic indices and drainage analysis. *Geoscience Frontiers*, 3(4), 407–428. <https://doi.org/10.1016/j.gsf.2011.12.002>
- Manjare, B. S. (2020). Morphotectonic Analysis of Upper Tapi River Sub-basin, Madhya Pradesh. *Journal of Geoscience Research*, 1(1), 81–88. <https://www.gondwanags.org.in/wp-content/uploads/2021/11/10-JGSR-Vol-1-1-Abstracts-Manajare.pdf>
- Ng, S. W.-P., Whitehouse, M. J., Roselee, M. H., Teschner, C., Murtadha, S., Oliver, G. J. H., Ghani, A. A., & Chang, S. C. (2017). Late Triassic granites from Bangka, Indonesia: A continuation of the Main Range granite province of the South-East Asian Tin Belt. *Journal of Asian Earth Sciences*, 138, 548–561. <https://doi.org/10.1016/j.jseaes.2017.03.002>
- Othman, A. T., & Omar, A. A. (2023). Evaluation of relative active tectonics by using geomorphic indices of the Bamo anticline, Zagros Fold-Thrust Belt, Kurdistan Region of Iraq. *Heliyon*, 9(7), e17970. <https://doi.org/10.1016/j.heliyon.2023.e17970>
- Partabian, A., Nourbakhsh, A., & Ameri, S. (2016). GIS-based evaluation of geomorphic response to tectonic activity in Makran Mountain Range, SE of Iran. *Geosciences Journal*, 20(6), 921–934. <https://doi.org/10.1007/s12303-016-0106-x>
- Saepuloh, A., Haeruddin, H., Heriawan, M. N., Kubo, T., Koike, K., & Malik, D. (2018). Application of lineament density extracted from dual orbit of synthetic aperture radar (SAR) images to detecting fluids paths in the Wayang Windu geothermal field (West Java, Indonesia). *Geothermics*, 72, 145–155. <https://doi.org/10.1016/j.geothermics.2017.11.010>
- Shiran, M., Asadi, M. A. Z., Mozzi, P., Adab, H., & Amirahmadi, A. (2020). Detection of surface anomalies through fractal analysis and their relation to morphotectonics (High Zagros belt, Iran). *Geosciences Journal*, 24(5), 597–613.

- <https://doi.org/10.1007/s12303-019-0042-7>
- Usman, E. (2016). the Geochemical Characteristic of Major Element of Granitoid of Natuna, Singkep, Bangka and Sibolga. *Bulletin of the Marine Geology*, 30(1), 45–54. <https://doi.org/10.32693/bomg.30.1.2015.74>
- Wang, Y., Qian, X., Zhang, Y., Gan, C., Zhang, A., Zhang, F., Feng, Q., Cawood, P. A., & Zhang, P. (2021). Southern extension of the Paleotethyan zone in SE Asia: Evidence from the Permo-Triassic granitoids in Malaysia and West Indonesia. *Lithos*, 398–399, 106336. <https://doi.org/10.1016/j.lithos.2021.106336>
- Zahirovic, S., Seton, M., & Müller, R. D. (2014). The Cretaceous and Cenozoic tectonic evolution of Southeast Asia. *Solid Earth*, 5(1), 227–273. <https://doi.org/10.5194/se-5-227-2014>
- Zhang, Y., Yu, X., Wang, Y., Qian, X., Gan, C., Ghani, A. A., Yu, Y., & Xu, C. (2023). Reconstructing the East Palaeo-Tethyan assemblage boundary in west Indonesia: constraints from Triassic granitoids in the Bangka and Belitung islands. *Geological Society, London, Special Publication*, 531, 265–286. <https://doi.org/10.1144/SP531-2022-144>
- Zhazhalayi, P. K., & Surdashy, A. (2022). Neo-tectonism and quantitative morphotectonic analysis of Roste Valley at imbricated-suture zones, Kurdistan Region, Iraq. *Iraqi Geological Journal*, 55(2E), 35–58. <https://doi.org/10.46717/igj.55.2E.3ms-2022-11-17>